MECHANICS 2025. Vol. 35. Issue 4. Pp. 619–642.

MSC2020: 70E60, 37N10, 76D05

© *A. V. Klekovkin, A. A. Chernova, Yu. L. Karavaev, A. V. Nazarov*

INVESTIGATION OF THE MOTION OF AN AQUATIC ROBOT WITH AN INTERNAL FAST-SPEED ROTOR AND A NONDEFORMABLE TAIL FIN

This paper reports on the simulation of the motion of an aquatic robot with an internal spinning rotor. We develop two mathematical models of robot motion in a fluid: the model of motion based on the Kirchhoff equations for the motion of a rigid body in a fluid and a model based on the Navier–Stokes equations. In addition to the simulation, we develop a prototype of the aquatic robot with a spinning rotor, with which we conduct real experiments. In this paper, we present the results of real experiments and simulations and draw conclusions based on them.

Keywords: aquatic robot, numerical simulation, finite-dimensional model, experimental investigations.

DOI: 10.35634/vm250407

Introduction

This paper is a continuation of a series of our previous publications on the motion of aquatic robots whose body is a nondeformable Joukowski foil which contains mechanisms that ensure changes in the position of the center of mass and/or changes in the angular momentum [17,23,24]. Despite a large number of studies in this area, this topic is of much current interest, and a number of open questions still remain concerning the completeness and correctness of mathematical models featuring the motion of a rigid body with internal mechanisms in a fluid. On the other hand, the interest in developing fairly simple mathematical models is motivated by the necessity of realizing, on their basis, control algorithms and control programs, which in practice have certain requirements concerning the speed of operation and computational complexity.

Mathematical models of physical processes that ensure the motion of an aquatic robot under periodic changes in the position of the center of mass and/or the internal angular momentum have not yet been fully verified in practice. In the early work on this topic the focus was on the motion of a nondeformable body in an ideal fluid, and the possibility of self-propulsion was characterized by the asymmetry of added masses and the periodicity of control (by displacement of the position of the center of mass or by changes in the internal angular momentum) [12,13,30,31]. In [4,6,20,35,40,44], the possibility of self-propulsion in the case of a viscous fluid was examined. In a number of publications, special attention was given to the motion of a nondeformable body in the presence of vortices [3, 21, 25, 39, 41]. In some recent papers, it was shown that the most efficient motion is achieved by ensuring a parametric resonance of the tail such that oscillations are transmitted from the robot body to the fluid [7, 8]. There are also known works that consider experimental prototypes that move in a fluid due to the movement of internal masses, including control algorithms [11, 16, 25, 33].

It should be noted that the principles of actuation under consideration are also used in combination with other mechanisms, for example, with a deformation of the shell [34], and when the actuation mechanisms are located outside the shells (bodies) submerged in a fluid [10, 26].

In this paper, we present two approaches to simulating the motion of an aquatic robot in a fluid. The first approach is based on the construction of a finite-dimensional model by analogy with Refs. [17, 23], but without taking into account the forces and torques generated during the deformation of the tail fin. To eliminate deformations, the tail fin had, in practice, a certain thickness, minimizing its deformations during motion. As shown in [2], one can achieve a better

fit of the solutions of this model based on ordinary differential equations to the real motion of a body in a fluid. The second approach is based on the numerical solution of the Navier–Stokes equations describing the fluid dynamics around a moving foil, which has allowed the velocity and the trajectory of the robot body to be reconstructed. To estimate the influence of the form of the robot body on the velocity of propulsion in the fluid, the investigations were carried out for different tail fin lengths. As a sample for comparison of the results of simulation of the approaches under consideration, full-scale experiments were conducted.

The main goal of the investigations is to compare two methods of mathematical simulation and to develop them further for describing the motion of more complex systems, namely, systems admitting or using the shell's deformation for their motion. In addition, this paper describes a new design of the aquatic robot with internal high-speed spinning rotor. To actuate the rotor one uses a high-speed brushless motor which makes it possible to accelerate the rotor to 20000 rev/min. This allows a considerable decrease in the mass of the system and an increase in the maneuverability. Research in this direction is motivated by the active development of combined robots (which combine different modes of motion in a fluid) and biosimilar robots, often with passive flexible fins [9, 11, 27], as well as mechanical systems with variable internal configurations [5].

§ 1. Mathematical model

1.1. Finite-dimensional model

Consider the plane-parallel motion of a body in a fluid. The shell of the body in the section is a symmetric NACA 0040 airfoil with chord $c = 200\,\text{mm}$. To describe the motion, we introduce two reference frames: a fixed (inertial) coordinate system $O'xy$ and a moving coordinate system rigidly attached to the body, Ox_1x_2 with origin at the center of mass of the robot's shell and with axis Ox_1 directed to the frontal part of the robot. We specify the position of point O by the radius vector $\boldsymbol{r} = (x, y)^T$ in the fixed coordinate system, and let α denote the turning angle between the axes Ox_1 and $O'x$, the positive direction of which is measured counterclockwise. A schematic representation of the robot with symbols denoting the coordinate systems is shown in Fig. 1.

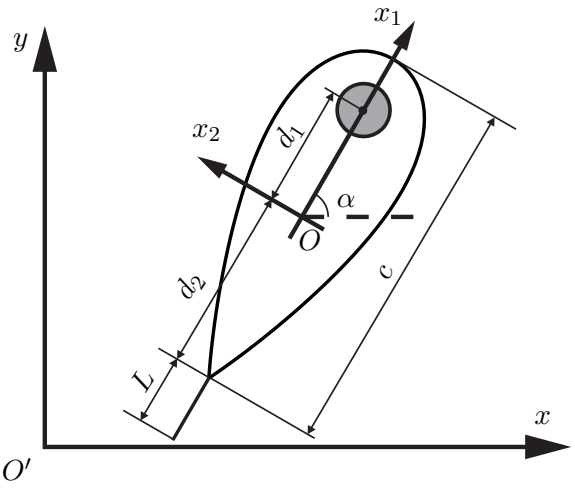

Fig. 1. A schematic representation of the aquatic robot with the shell of the form of the NACA 0040 foil with chord c, where $O'xy$ and Ox_1x_2 are the fixed coordinate system and the moving coordinate system, respectively, α is the turning angle of the moving coordinate system relative to the fixed coordinate system, d_1 is the distance from the origin of the moving coordinate system to the center of mass of the rotor, d_2 is the distance from the origin of the moving coordinate system to the point of attachment of tail fins, and L is the length of the tail fin

The shell contains an axisymmetric rotor, which can rotate about the axis passing through its center of mass. The center of mass of the rotor lies on the axis Ox_1 at distance d_1 from the origin of the moving coordinate system.

A passive rigid tail fin of length L is fastened to the shell of the robot at the rear end, and its attachment point lies on the axis Ox_1 at distance d_2 from the origin of the moving coordinate system. In the description of motion, we assume the robot body with the tail to be nondeformable. In the course of experiments, the length of the tail, L, was varied.

To describe the motion, we introduce a vector of generalized coordinates $\boldsymbol{q} = (x, y, \alpha)^T$ and a vector of quasi-velocities $\boldsymbol{w} = (v_1, v_2, \omega)^T$, where v_1 and v_2 denote the projections of the linear velocity of the center of mass of the robot onto the moving axes and ω is the angular velocity of the body. The equations of motion for this body can be written in terms of the Kirchhoff equations supplemented with viscous resistance terms [17]:

$$\begin{gathered} \mathbf{A}(\boldsymbol{w})\dot{\boldsymbol{w}} + \mathbf{B}(\boldsymbol{w})\boldsymbol{w} + \mathbf{C}(\boldsymbol{w})\boldsymbol{w} + \boldsymbol{u}_c = 0, \\ \boldsymbol{q} = \mathbf{R}(\boldsymbol{q})\boldsymbol{w}; \end{gathered} \tag{1.1}$$

where the matrices $\mathbf{R}(\boldsymbol{q})$, $\mathbf{A}(\boldsymbol{w})$, $\mathbf{B}(\boldsymbol{w})$ and $\mathbf{C}(\boldsymbol{w})$ and the vector $\boldsymbol{u}_c$ have the form

$$\mathbf{R}(\boldsymbol{q}) = \begin{pmatrix} \cos\alpha & -\sin\alpha & 0 \\ \sin\alpha & \cos\alpha & 0 \\ 0 & 0 & 1 \end{pmatrix}, \quad \mathbf{A}(\boldsymbol{w}) = \begin{pmatrix} m_s + \lambda_{11} & 0 & 0 \\ 0 & m_s + \lambda_{22} & d_1 m_r + \lambda_{23} \\ 0 & d_1 m_r + \lambda_{23} & I + \lambda_{33} \end{pmatrix},$$

$$\mathbf{B}(\boldsymbol{w}) = \begin{pmatrix} 0 & -(m_s + \lambda_{22})\omega & -(d_1 m_r + \lambda_{23})\omega \\ (m_s + \lambda_{11})\omega & 0 & 0 \\ (d_1 m_r + \lambda_{23})\omega & (\lambda_{22} - \lambda_{11})v_1 & 0 \end{pmatrix},$$

$$\mathbf{C}(\boldsymbol{w}) = \begin{pmatrix} c_1|v_1| + c_1 & 0 & 0 \\ 0 & c_2|v_2| + c_2 & 0 \\ 0 & 0 & c_{3sq}|\omega| + c_{3lin} \end{pmatrix}, \quad \boldsymbol{u}_c = \begin{pmatrix} 0 \\ 0 \\ I_r\dot{\Omega} \end{pmatrix},$$

$$m_s = m_b + m_r, \quad I = I_b + I_r + m_r d_1^2.$$

where m_b is the mass of the shell, m_r is the mass of the rotor, I_b is the moment of inertia of the shell relative to the vertical axis passing through its center of mass, I_r is the moment of inertia of the rotor, $c_1, c_2, c_{3sq}, c_{3lin}$ are the coefficients of viscous resistance, and $\lambda_{11}, \lambda_{22}, \lambda_{23}, \lambda_{33}$ are the coefficients of added masses.

In equations (1.1), the hydrodynamic forces acting on the body have been taken into account using the effect of added masses (the inertial component of the hydrodynamic forces) and the viscous resistance of the fluid. Note that the viscous resistance is described by using a combination of linear and quadratic dependences. This form of description of viscous resistance is used in recent works where modeling of aquatic robots is considered [18, 45], however, this idea goes back to Huygens [1]. If we admit an approximation of the form of the robot by an elliptic cylinder with a major semiaxis a, with a minor semiaxis b and height h (meaning the height of the part of the robot submerged in the fluid), then the coefficients $c_1, c_2, c_{3sq}, c_{3lin}$ can be calculated using the following expressions [18]:

$$c_1 = \frac{1}{2}\rho\pi C_f \frac{b+a}{2}h, \qquad c_2 = \frac{1}{2}\rho C_d 2ah,$$

$$c_{3sq} = \frac{1}{8}\rho\pi C_f (a+b)h^4, \quad c_{3lin} = \frac{1}{6}\rho\pi C_f (a+b)h^3,$$

where ρ is the fluid density, and C_f and C_d are the dimensionless coefficients of viscous resistance whose choice will be described below.

To calculate the coefficients of added masses, one can find expressions in the literature for an elliptic contour with a prominent edge that has a major semiaxis a, a minor semiaxis b and an edge of length L [29]:

$$\lambda'_{11} = \rho\pi C_A b^2, \qquad \lambda'_{22} = \frac{1}{4}\rho\pi C_A a^2 \left[(m+1)^2 \left(1+\frac{b}{a}\right)^2 - \frac{4b}{a}\left(2+\frac{b}{a}\right)\right],$$

$$\lambda'_{33} = \frac{1}{2^7}\rho\pi C_A (a+b)^2 \left[(a+b)^2 \left(9m^4+4m^3-10m^2+4m-7\right) + 16\,(a-b)^2\right],$$

$$\lambda'_{23} = \frac{1}{8}\rho\pi C_A a^3 \left(1+\frac{b}{a}\right)^3 \left(m^2-1\right)(m+1),$$

$$m = \frac{a+L}{a+b} + \frac{b}{a+L+\sqrt{b^2+L^2+2aL}},$$

where C_A is the dimensionless coefficient depending on the modes of motion, wave formation, and the presence of a free fluid surface, a bottom or of rigid walls etc. near the object.

At this point it should be noted that the coefficient λ_{23} of the elliptic contour without a prominent edge (with $L = 0$) vanishes, whereas the airfoil has the coefficient $\lambda_{23} \neq 0$ even in the absence of a tail (there is no transverse axis of symmetry). Therefore, in this paper we first calculate the coefficient λ^0_{23} for a symmetric Joukowski foil with similar dimensions with the NACA 0040 foil using the following expressions [29]:

$$\lambda^0_{23} = \frac{1}{8}\rho\pi C_A p^3 \left(r^3 + R^3 + r^2 + R^2 + 2(r+R)\right),$$

$$\mu = (1.54b/c)/(1-1.2b/c), \qquad p = \frac{c}{2(1+\mu^2)}, \qquad R = 1+\mu, \qquad r = \frac{1+\mu}{1+2\mu}.$$

In simulating the motion of the robot, we will calculate the coefficients of added masses from the following expressions:

$$\lambda_{11} = \lambda'_{11}h, \qquad \lambda_{22} = \lambda'_{22}h, \qquad \lambda_{33} = \lambda'_{33}h, \qquad \lambda_{23} = h(\lambda^0_{23} + \lambda'_{23}),$$

where h is the depth of submersion of the robot.

The values of the mass-inertial parameters in the simulation correspond to the parameters of the prototype developed for experimental investigations (it is described below). The values of the other parameters were taken to be:

$$C_f = 0.011, \qquad C_A = 0.5,$$

$$c = 0.2, \qquad a = \frac{1}{2}c + \frac{1}{2}L, \qquad b = 0.04, \qquad h = 0.06,$$

where the coefficient of longitudinal viscous resistance C_f and the coefficient of added masses C_A were chosen in accordance with the general recommendations [14, 15, 18, 32, 45], whereas the value of the transverse viscous coefficient of resistance C_d increases with increasing ratio a/b (a and b are the semiaxes of the ellipse to which the boat's foil approaches). It is found experimentally that the motion occurs at Reynolds numbers $\mathrm{Re} < 10^5$. Accordingly, we choose values of C_d for different tail fin lengths, which are summarized in Table 1:

Table 1. The value of the coefficient of transverse resistance C_d depending on the chosen tail

Length of the tail fin, L, mm	0	35	70	105
C_d	1.5	2.2	2.4	2.5

1.2. Numerical simulation based on the solution of the Navier–Stokes equations

To formulate the problem of numerical simulation based on the solution of the Navier–Stokes equations, we will consider the motion of a drop-shaped body (Fig. 2) in an incompressible viscous fluid.

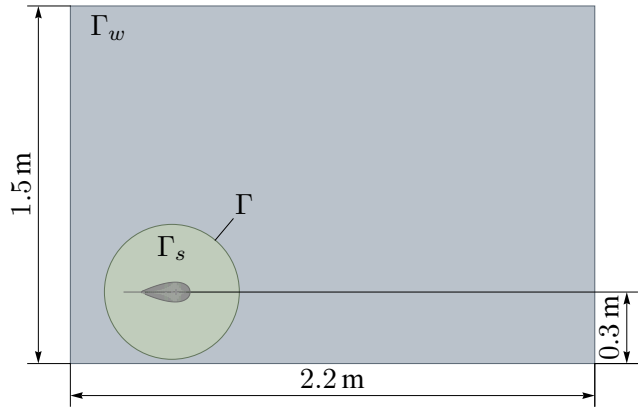

Fig. 2. Computational domain

In the first approximation, we consider the problem in a planar setting. In this case, it is appropriate to make the following assumptions: the action of the gravity force and the buoyancy force are balanced and are ignored in the problem statement; we consider an internal fluid layer that has no interface (i. e., we do not consider the presence and influence of the free surface on the dynamics of the fluid and the moving object); the fluid is assumed to be isotropic and isothermal, and the system as a whole is assumed to be isolated (the processes of heat exchange are not considered); the drop-shaped body is defined as a rigid absolutely smooth body (i. e., the roughness is not considered).

To combine the physical subproblems of fluid dynamics and those of the motion of a drop-shaped body in a fluid into one problem, it is necessary to formulate additional kinematic and dynamic boundary conditions on contact surfaces. Next, we will use the symbols Γ_w and Γ_s to refer only to the subregions occupied by the fluid and the drop-shaped body, respectively, and the symbol Γ to denote the boundaries of the body's contact with the fluid (the lateral surface of the body).

The formulation of additional kinematic and dynamic boundary conditions on contact surfaces in the case of a description of a dynamically changing boundary of a waterproof solid body-fluid contact requires determining the equality of the velocities and accelerations of the body to the velocities and accelerations of the fluid at the contact boundary. Therefore, the conditions at the initial time t_0 can be defined as:

$$\begin{aligned} \dot{\mathbf{u}}_s(t_0) &= \dot{\mathbf{U}}_w(t_0), \\ \ddot{\mathbf{u}}_s(t_0) &= \ddot{\mathbf{U}}_w(t_0) \end{aligned} \tag{1.2}$$

where $\mathbf{u}_s(t)$ are movements of the drop-shaped body and $\mathbf{U}_w(t)$ are movements of the fluid.

The conditions for dynamical compatibility take the form

$$p_s \mathbf{n}_s = p_w \mathbf{n}_w, \tag{1.3}$$

where p_s is the pressure of a drop-shaped body on a fluid, p_w is the pressure of fluid on a drop-shaped body; $\mathbf{n}_s, \mathbf{n}_w$ are the external normals ($\mathbf{n}_s = -\mathbf{n}_g$).

With the above assumptions and equations (1.2), (1.3) in mind, the fluid dynamics can be defined by the system of Navier–Stokes equations:

$$\begin{array}{l} \nabla \cdot \mathbf{u} = 0, \\ \frac{\partial \rho \mathbf{u}}{\partial t} + \mathbf{u} \cdot \nabla \rho \mathbf{u} = -\nabla p + \nabla \cdot \tau \end{array} \tag{1.4}$$

where ρ is the fluid density ($\rho = 1000$ kg/m^3), p is the pressure, $\tau = \mu(\nabla \mathbf{u} + \nabla \mathbf{u}^{\mathbf{T}})$ is the tensor field of viscous stresses, and $\mu = 1 \cdot 10^{-6}$ Pa· s is the coefficient of dynamical fluid viscosity.

The system (1.4) is closed by the state equation $\rho = \text{const}$. The boundary conditions are defined as follows:

- for the impermeable solid heat-insulated wall (the external boundaries of the reservoir bounding the fluid on the left, at the front and behind): $\mathbf{U}_w = 0$;
- on the boundary of the contact Γ the velocity of the fluid coincides with the linear velocity of the body: $\mathbf{U}_w = \mathbf{u}_s$.

The initial conditions can be defined for the fluid as: $\mathbf{U}_w = 0$ m/s, $p = 1$ atm.

The oscillations of the rotor are given by the function $\Omega(t)$, the form of which agrees with that observed in the experiment and is described below. Then, the control function for the drop-shaped body–fluid system will be the derivative of the gyrostatic momentum:

$$\dot{K}(t) = I_r \dot{\Omega}(t), \tag{1.5}$$

where $I_r = 3.6 \cdot 10^{-6}$ kg ·m ^{2} is the axial moment of inertia of the rotor.

Taking (1.5) into account, the equation of moments of forces acting on a drop-shaped body can be written as

$$M_{comp} = M_{water} - \dot{K}, \tag{1.6}$$

where M_{comp} is the total torque and M_{water} is the moment of hydrodynamic forces.

For the drop-shaped body: $\mathbf{u}_s = \begin{pmatrix} 0.002 \\ 0 \\ 0 \end{pmatrix}$; $\dot{\mathbf{u}}_s = 0$; $\Omega = 0$; $\dot{\Omega} = 0$.

The solution of the problem (1.4)–(1.6), with the compatibility conditions (1.2)–(1.3) taken into account, will be constructed numerically using the method of control volumes. The control volume is constructed around each grid node (as an example, a flat triangular grid element is considered) using a median dyad (it is defined by lines connecting the centers of the ribs and the centers of the elements (edges) around the node).

The construction of the method of control volumes using the equations of conservation of mass, moments and some passive scalar can be represented in the following form.

1. Determining the center of the control volume C:

$$\int_{V_C} \left(\mathbf{r} - \mathbf{r}_C\right) dV = 0.$$

2. The initial partial differential equations

$$\frac{\partial \rho}{\partial t} + \frac{\partial}{\partial x_j}\left(\rho U_j\right) = 0,$$

$$\frac{\partial}{\partial t}(\rho U_i) + \frac{\partial}{\partial x_j}\left(\rho U_j U_i\right) = -\frac{\partial p}{\partial x_i} + \frac{\partial}{\partial x_j}\left(\mu\left(\frac{\partial U_i}{\partial x_j} + \frac{\partial U_j}{\partial x_i}\right)\right),$$

$$\frac{\partial}{\partial t}(\rho\phi) + \frac{\partial}{\partial x_j}(\rho U_j \phi) = \frac{\partial}{\partial x_j}\left(\Gamma\left(\frac{\partial \phi}{\partial x_j}\right)\right) + S_\phi$$

are integrated over each control volume.

3. The application of the Ostrogradskii–Gauss theorem leads to the form

$$\frac{d}{dt}\int_V \rho\,dV + \oint_S \rho U_j\,dn_j = 0,$$
$$\frac{d}{dt}\int_V \rho U_i\,dV + \oint_S \rho U_j U_i\,dn_j = -\oint_S p\,dn_j + \oint_S \mu\left(\frac{\partial U_i}{\partial x_j}\right)dn_j + \int_V S_{U_i}\,dV, \tag{1.7}$$
$$\frac{d}{dt}\int_V \rho\phi\,dV + \oint_S \rho U_j\phi\,dn_j = \oint_S \Gamma\left(\frac{\partial \phi}{\partial x_j}\right)dn_j + \int_V S_\phi\,dV,$$

where V and S are the volume and surface domains of integration.

4. Next, it is necessary to discretize the volume and surface integrals. The volume integrals are discretized within each sector of the element and are summed in the control volume to which the sector belongs. The surface integrals are discretized at the points of integration i_{pn} (Fig. 3).

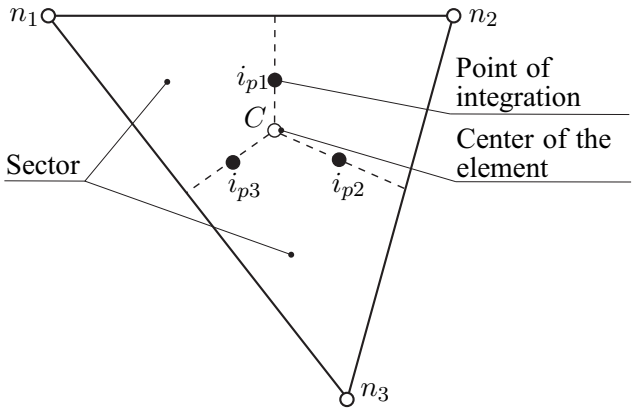

Fig. 3. Grid element

After discretizing the volume and surface integrals, the discretized equations take the form

$$V\left(\frac{\rho-\rho^0}{\Delta t}\right) + \sum_{ip}(\rho U_j \Delta n_i)_{ip} = 0,$$
$$V\left(\frac{\rho_i U_i - \rho^0 U_i^0}{\Delta t}\right) + \sum_{ip}(\rho U_j \Delta n_i)_{ip}(U_i)_{ip} = \sum_{ip}(p\Delta n_i)_{ip} +$$
$$+\sum_{ip}\left(\mu\left(\frac{\partial U_i}{\partial x_j}+\frac{\partial U_j}{\partial x_i}\right)\Delta n_j\right)_{ip} + \bar{S_{U_i}}V,$$
$$V\left(\frac{\rho\phi-\rho^0\phi^0}{\Delta t}\right) + \sum_{ip}(\rho U_j \Delta n_i)_{ip}\phi_{ip} = \sum_{op}\left(\Gamma\frac{\partial\phi}{\partial x_j}\Delta n_j\right)_{ip} + \bar{S}_\phi V,$$

where V is the control volume, Δt is the time step, Δn_i is the discrete external surface vector, the subscript ip denotes the estimate at the point of integration, the summation is over all points of integration of the control volume, and the superscript "0" denotes the preceding time step.

During the transition from the initial computational domain to its discretized form, a change of surface integrals is made by summation over the edges of the test cells, and the form of approximation of the integrands is determined by the specific numerical scheme used.

The gradient in the test cell can be defined as

$$\nabla\phi_i = \frac{1}{V_i}\sum_j \mathbf{n}_{ij}s_{ij}\phi_{ij},$$

where V_i is the size of the ith cell, s_{ij} is the edge between the ith and the jth cells of the grid, $\mathbf{n}_{ij}$ is the unit vector of the external normal to the edge s_{ij}, and ϕ_{ij} is the value of ϕ at the ijth edge; ϕ_{ij} determined by linear interpolation.

The gradients at the edge between the cells are calculated by linear interpolation of the gradients from cells i and j — $\overline{\nabla(\phi)_{ij}}$.

The divergence is calculated by the formula

$$\nabla\cdot\left(\phi_i\mathbf{U}_i\right) = \frac{1}{U_i}\sum_j s_{ij}\mathbf{n}_{ij}\cdot\mathbf{U}_{ij}\phi_{ij}.$$

The approximation of diffusion terms is constructed as follows:

$$\nabla\cdot\Gamma\nabla\phi = \frac{1}{V_i}\sum_j \Gamma_{ij}\mathbf{s}_{ij}\cdot\nabla\phi_{ij},$$

where Γ_{ij} is the coefficient of diffusion at the edge ij.

To discretize convective terms, we use the scheme of central differences of the form

$$\phi_{ip} = \phi_{up} + \beta\nabla\phi\cdot\vec{r},$$

where ϕ_{ip} is the sought-for convective stream determined through the values of the convective stream ϕ at the nodal points of the computational grid, ϕ_{up} is the value of the convective stream at the node located against the stream, $\vec{r}$ is the vector lowered from the angle of the grid lying against the stream to the point where the coefficient $\beta \approx 1$ is determined locally with minimization of local oscillations of solutions and is calculated separately for each component of the vector, and $\nabla\phi$ is the value of the convective stream at the node located against the stream.

The approximation of diffusion terms of the conservation equations is constructed using the functions of forms. For example, for the derivative in the direction x at the point of integration ip:

$$\left.\frac{\partial\phi}{\partial x}\right|_{ip} = \sum_n \left.\frac{\partial N_n}{\partial x}\right|_{ip}\phi_n.$$

The summation is over all functions of the form for the element, and the derivatives of the functions of the form with respect to the Cartesian coordinates can be expressed in terms of their local derivatives using the matrix of Jacobi transformations:

$$\begin{bmatrix}\frac{\partial N}{\partial x}\\ \frac{\partial N}{\partial y}\\ \frac{\partial N}{\partial z}\end{bmatrix} = \begin{bmatrix}\frac{\partial x}{\partial s} & \frac{\partial y}{\partial s} & \frac{\partial z}{\partial s}\\ \frac{\partial x}{\partial t} & \frac{\partial y}{\partial t} & \frac{\partial z}{\partial t}\\ \frac{\partial x}{\partial u} & \frac{\partial y}{\partial u} & \frac{\partial z}{\partial u}\end{bmatrix}^{-1}\begin{bmatrix}\frac{\partial N}{\partial s}\\ \frac{\partial N}{\partial t}\\ \frac{\partial N}{\partial u}\end{bmatrix}.$$

The estimate of the gradients of the function of the form is constructed on the basis of trilinear interpolation.

The resulting system of difference equations is solved by the method of conjugate gradients. To accelerate its convergence, the algebraic multigrid method [37] is used.

It should be noted that, as the computational grids were constructed, the drop-shaped rigid body with a motor inside was cut from the computational domain. The pseudo-two-dimensional computational grid for the fluid (Fig. 4) included 120000 hexahedral cells.

The solution of conjugate problems was constructed in a strongly coupled formulation [28] using 50 iterations in each time step for a correct transfer of the position of the body in a fluid from the subproblem of the dynamics of a body to the hydrodynamics and transmission of the resistance forces arising in the fluid (the hydrodynamic force and torques) to the body. Also,

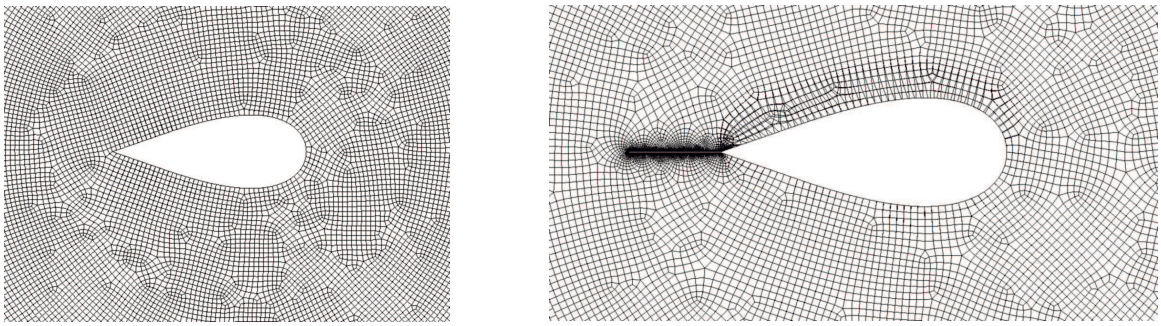

(a) (b)

Fig. 4. Fragment of a computational grid near the boundary Γ for a body without a tail (a) and a body with a tail 2 mm in thickness (b)

the motion of the rigid body was determined by the forces and the torque acting on the body. The algorithm for solving the problem of body motion due to the change in the internal masses involves application of Newmark's linear scheme for calculation of the straight-line motion and the application of the Simo-Wong agorithm [36] for the rotational motion of the rigid body. The deformation of the grid and correction of equations (1.7) are performed in accordance with the Leibniz rule (differentiation of the integral by parameter) with control of the velocity of change in the deformable control volume and correctness of the advective transfer through the moving boundaries of the control volume.

By solving the problem under consideration we have obtained both the fluid velocity and pressure fields for each time instant of the interval considered, the trajectories of the drop-shaped body in the fluid and the dependences of changes in the hydrodynamic force and torques which arise at the boundary Γ in time.

§ 2. Description of the design of the prototype of an aquatic robot

To verify the developed mathematical models described in Sections 1.1 and 1.2, an experimental prototype of the aquatic robot was created. The robot body was made using a 3D-printer of PLA-plastic and has in the section the form of an airfoil with overall dimensions 200 x 80 x 80 mm (without taking the tail fin into account) and a wall thickness of 2.5 mm. The tail of the robot body is designed to have guides for fast change of tail fins. The lower part of the robot body is designed to have two openings for pins on which a platform with a spinning rotor and a control board is installed. A photograph of the prototype of the robot is shown in Fig. 5.

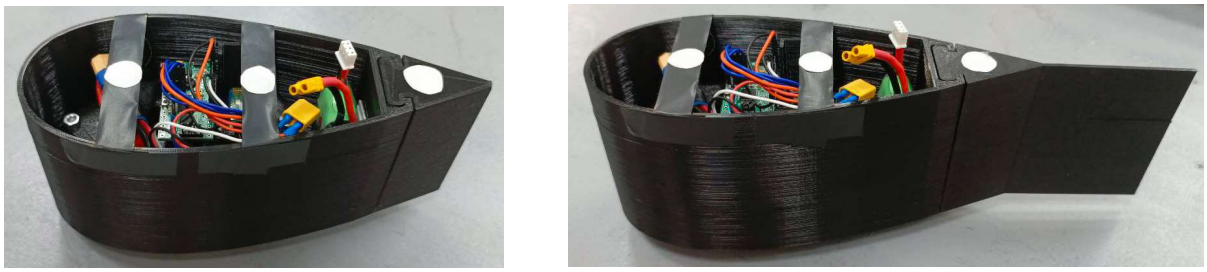

(a) (b)

Fig. 5. A prototype of the developed robot: a) with a tail insert without a tail fin, b) with a tail fin installed on it

The fast-revolving rotor is a steel cylinder with overall dimensions 30 x 6 mm and a mass of 33 g, which is placed on the shaft of the brushless direct current motor (the characteristics of

the motor are presented in Table 2). The rotor is installed on the platform in such a way that its axis of rotation is on the symmetry axis of the robot body, and the center of mass of the entire platform is as close as possible to the lower part of the robot body. The platform also has an original control board based on the STM32F103C8T6 microcontroller, a control board for the driver of the brushless motor and a LiPo storage battery, with a rated voltage of 7.4 V. The 3D-model of the robot body with the main internal elements is shown in Fig. 6.

Table 2. Characteristics of the brushless direct current motor

Characteristic	Value
KV	2450
Interfacial resistance	46.8 MOm
Peak current	42.63 A
Maximal power	682.1 W
Configuration of the motor	12N14P

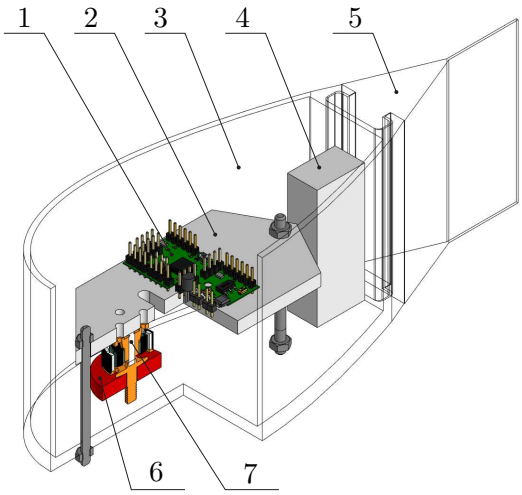

Fig. 6. 3D-model of the robot body: 1 is the control board; 2 is the internal platform; 3 is the robot body; 4 is the storage battery; 5 is the tail fin; 6 is the rotor; 7 is the motor

The parameter values of the prototype are summarized in Table 3.

The robot is designed to have tail fins of different forms and sizes. A photograph of tail fins installed on the robot within the framework of the study is shown in Fig. 7, a, b. For example, when the leftmost tail (see Fig. 7, a, b) is installed, the robot body becomes wing-shaped and has a sharp edge. The other tails have been made so that they have the same thickness of the tail fin (2 mm) and different lengths. Since the motion models assume that the tail is nondeformable, the chosen thickness guarantees a sufficient rigidity of the tail fin. All tails used were fabricated using a 3D-printer.

§ 3. Comparison of the results of experimental and theoretical investigations

3.1. Description of the methods for conducting the experiment

The developed prototype of the aquatic robot enables motion by periodic rotation of the rotor with different angular velocities, which are control actions. The form of the control action was

Table 3. Mass-geometric parameters of the prototype

Characteristic	**Notation**	**Value**
Mass of the shell of the robot	m_b	0.41 kg
Moment of inertia of the shell of the robot	I_b	0.007468 kg·m^2
Mass of the rotating rotor	m_r	0.033 kg
Distance from the center of mass of the robot body to the axis of rotation of the rotor	d_1	0.02 m
Distance from the center of mass of the robot body to the point of attachment of the tail fin	d_2	0.12 m
Moment of inertia of the rotor	I_r	0.000004 kg·m^2
Maximal velocity of rotation of the rotor	$\Omega_{\max}$	20090 rev/min

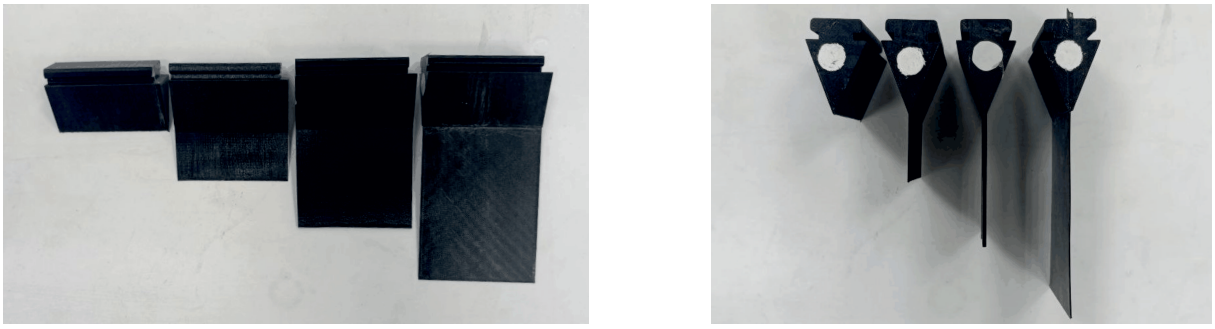

(a) (б)

Fig. 7. Photograph of tail fins with dimensions $L = 0; 35; 70; 105$ mm, respectively

given by analogy with Refs. [17, 22, 23], where the angular velocity of the rotor is a periodic piecewise-linear function:

$$\Omega(t) = \begin{cases} \Omega_{\max} & t \in [nT; nT + t_1)\,, \\ \tau_1 t - \tau_2 t & t \in [nT + t_1; nT + t_1 + t_{\text{acc}})\,, \\ 0 & t \in [nT + t_1 + t_{\text{acc}}; nT + t_1 + t_3 + t_{\text{acc}})\,, \\ \tau_1 t - \tau_3 & t \in [nT + t_1 + t_3 + t_{\text{acc}}; T(n+1))\,, \end{cases} \tag{3.1}$$

where $\tau_1 = \dfrac{\Omega_{\max}}{t_{\text{acc}}}$, $\tau_2 = \dfrac{\Omega_{\max}(t_1 + nT + t_{\text{acc}})}{t_{\text{acc}}}$, $\tau_3 = \dfrac{\Omega_{\max}(T + nT + t_{\text{acc}})}{t_{\text{acc}}}$, $n = 0, 1, 2, 3, \ldots$, $\Omega_{\max}$ is the maximal velocity of rotation of the rotor, T is the period of the control signal, t_1 and t_3 are the time of rotation of the rotor with constant velocity, t_{acc} is the time it takes the rotor to change its velocity from 0 to $\Omega_{\max}$ rad/s (this motor accelerates the rotor from 0 to $\Omega_{\max}$ rad/s and decelerates the rotor from the velocity $\Omega_{\max}$ rad/s to 0 within the same time). For the developed prototype the value $t_{\text{acc}} = 0.5$ s. Taking into account the time of acceleration of the rotor, for a control action of the form (3.1), we set the minimal period of the control action to be $T = 1.2$ s. In all experiments presented above, the motor rotated in its maximal range from 0 to 20090 rev/min. The robot started moving from rest.

To conduct experiments with the developed prototype of the aquatic robot, a pool with dimensions 2 m x 1.2 m was used. The tracking of the trajectory of the robot was performed using the Brio Ultra HD Pro camera (30 frames per minute). Video recording was performed in the program Logitech Capture. Analysis of the video data obtained and tracking the markers fastened on the robot body were performed using specialized software. Each experiment was repeated at

least three times. The velocities were calculated using numerical differentiation and a moving average filter.

Figure 8 shows a frame with a typical trajectory of the experimental prototype and graphs with the trajectory of motion with different tail fins with the period of control action $T = 1.2$ s.

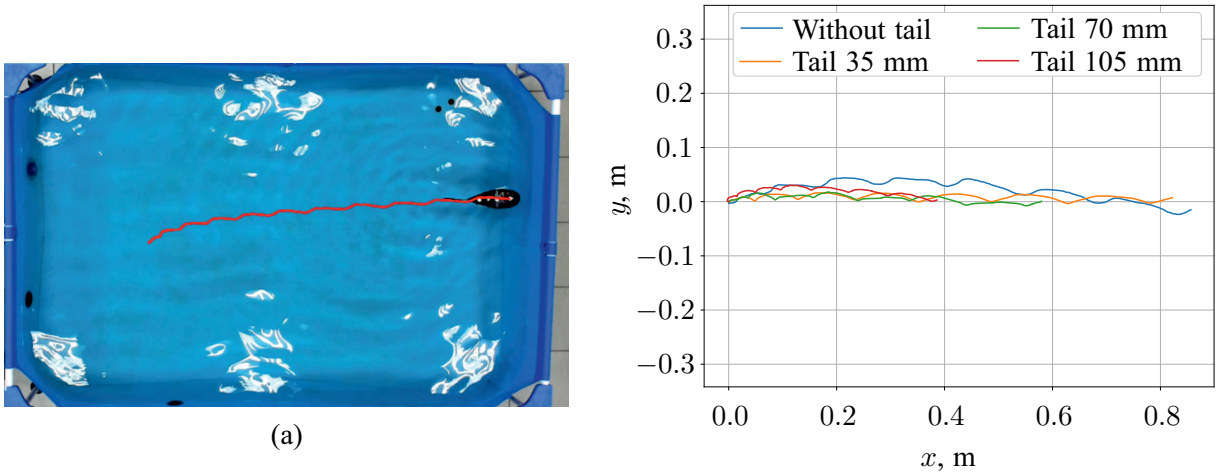

(a) (b)

Fig. 8. a) Frame with the trajectory of motion; b) experimental trajectories of the robot with developed tails

Figure 9 shows the trajectories and the longitudinal velocities for the robot with a tail fin of length 35 mm and the period of control action $T = 1.2$ s, obtained from the experiment and from simulations.

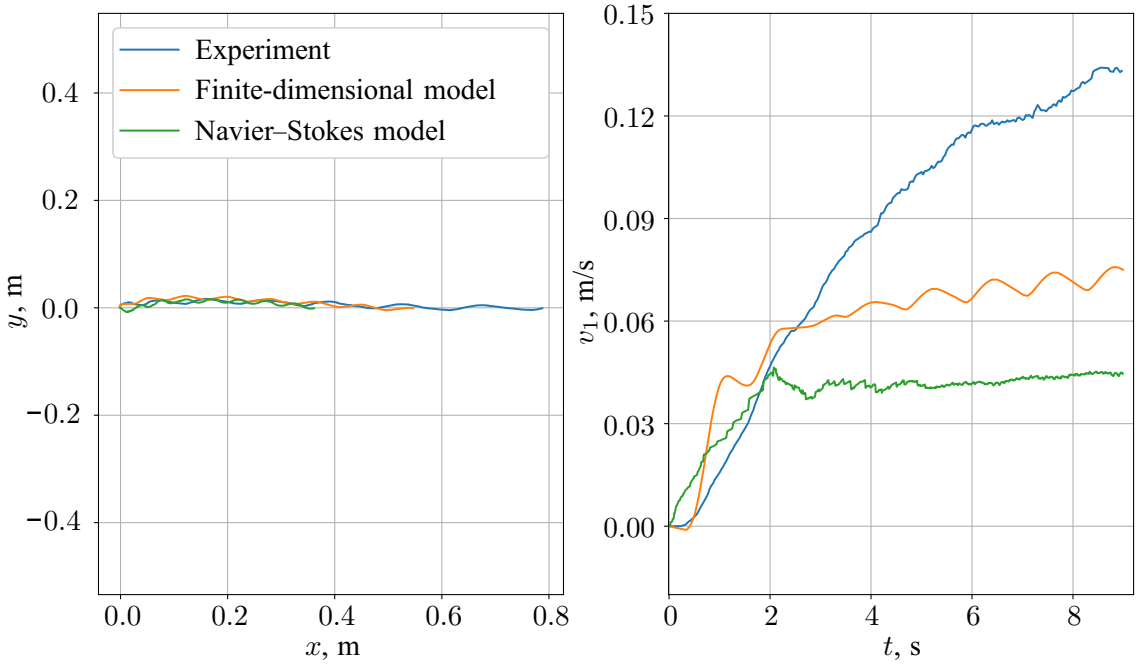

Fig. 9. Trajectories and velocities of the robot in the experiment and simulations with the period of control action $T = 1.2$ s and a tail fin of length 35 mm

From the graphs in Fig. 9 it can be seen that, on average, the robot moves in a straight line with periodic oscillations in the transverse direction, both in the experiment and in simulations. In

the simulations, the linear velocities of the robot have a smaller value than the velocity reached in the experiment. Next, we consider a similar experiment, but with the period of the control signal $T = 3$ s (see Fig. 10).

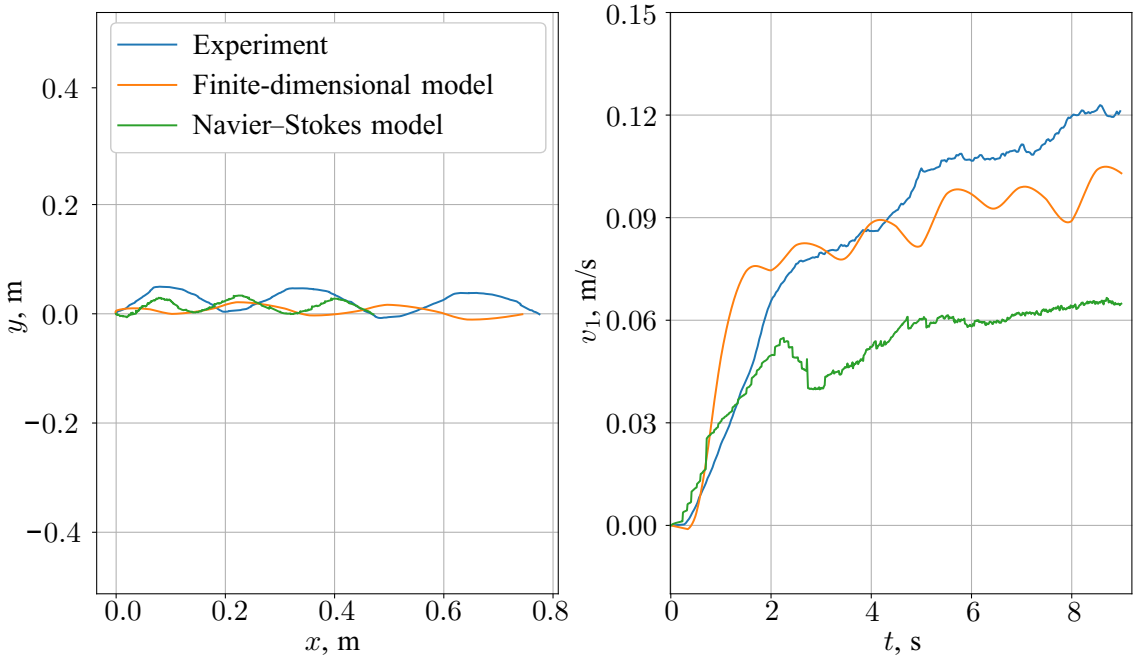

Fig. 10. Trajectories and velocities of the robot in the experiment and simulation with the period of control action $T = 3$ s and a tail fin length of 35 mm

From the graphs in Fig. 10 it can be seen that, as compared to the experiment for period $T = 1.2$ s, in the experiment with period $T = 3$ s the distance traveled did almost not change. It was only the amplitude of transverse oscillations that increased during motion. The linear velocity of the robot did almost not change in the experiment either. But in the simulation (for both models), the velocity became closer to the experimental one, and in the finite-dimensional model it is almost the same as that observed in the experiment, which can also be seen from the distance covered by the robot.

Consider the influence of the length of the tail fin on the propulsion of the robot. Figure 11 shows the trajectories and Figure 12 shows the longitudinal linear velocities of the robot obtained from the experiments and the results of numerical simulations within the framework of the developed mathematical models (the finite-dimensional model of motion and the model based on the Navier–Stokes equations) for each of the tails. The period of control action is $T = 1.2$ s, the duration of the robot motion is 9 seconds in each experiment. Also, analogous graphs have been obtained for the period of the control signal $T = 3$ s (see Fig. 13 and Fig. 14).

From the experiments with control period $T = 1.2$ s one can draw the conclusion that, with increasing tail length, the velocity of the robot decreases. However, it can be clearly seen from the results with control period $T = 3$ s that in the experiment the velocity of the robot without a tail fin is smaller than the velocity of the robot with a tail fin of length $L = 35$ mm and is almost equal to the velocity of the robot with a tail fin $L = 70$ mm. This phenomenon is also observed in the simulation results, but to a lesser extent.

We consider in more detail the influence of the period of the control signal on the linear velocity of the robot. To this end, we conduct experiments with control periods $T = 1.0$; 1.2; 1.4; 1.6; 1.8; 2.0; 2.5; 3.0; 3.5; 4.0 s. In the simulations for this experiment we used only a finite-dimensional model as it allowed us to obtain results qualitatively similar to those of the real

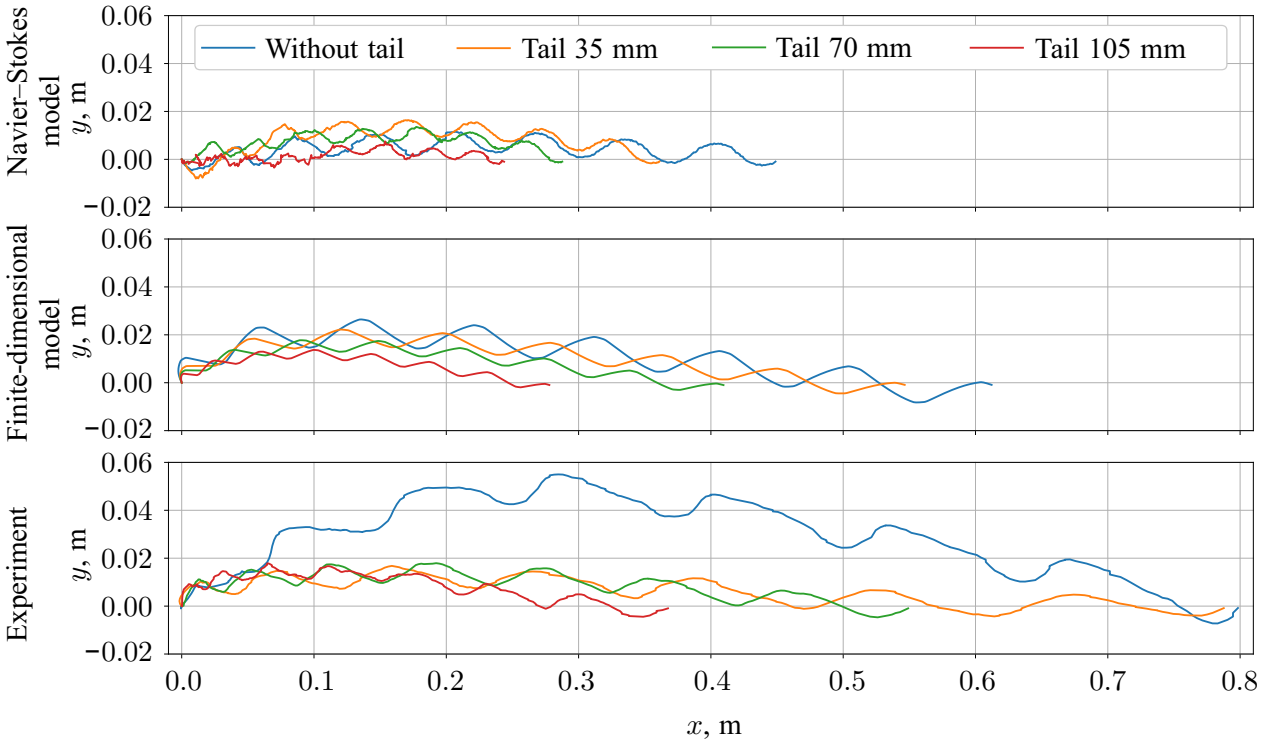

Fig. 11. Trajectories of the robot in the experiment and simulations with the period of control action $T = 1.2$ s for different tail fins

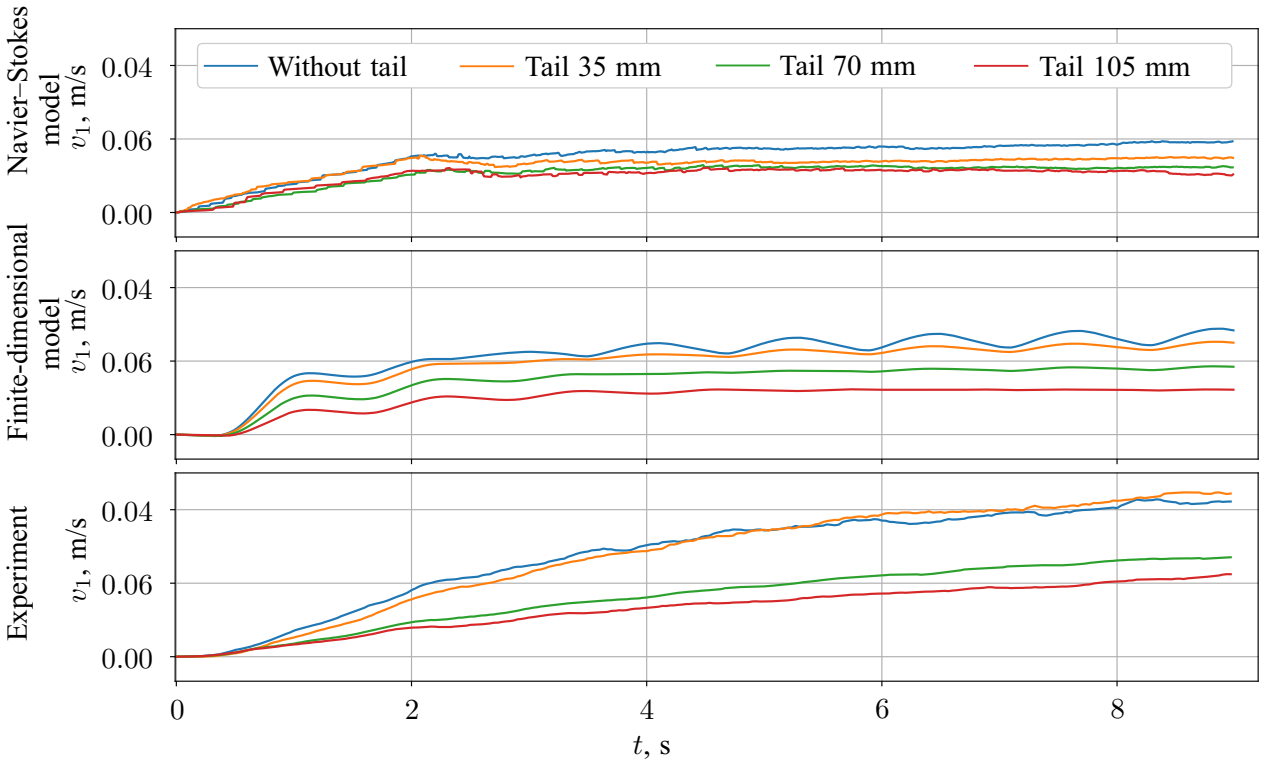

Fig. 12. Linear velocities of the robot in the experiment and simulations with the period of control action $T = 1.2$ s for different tail fins

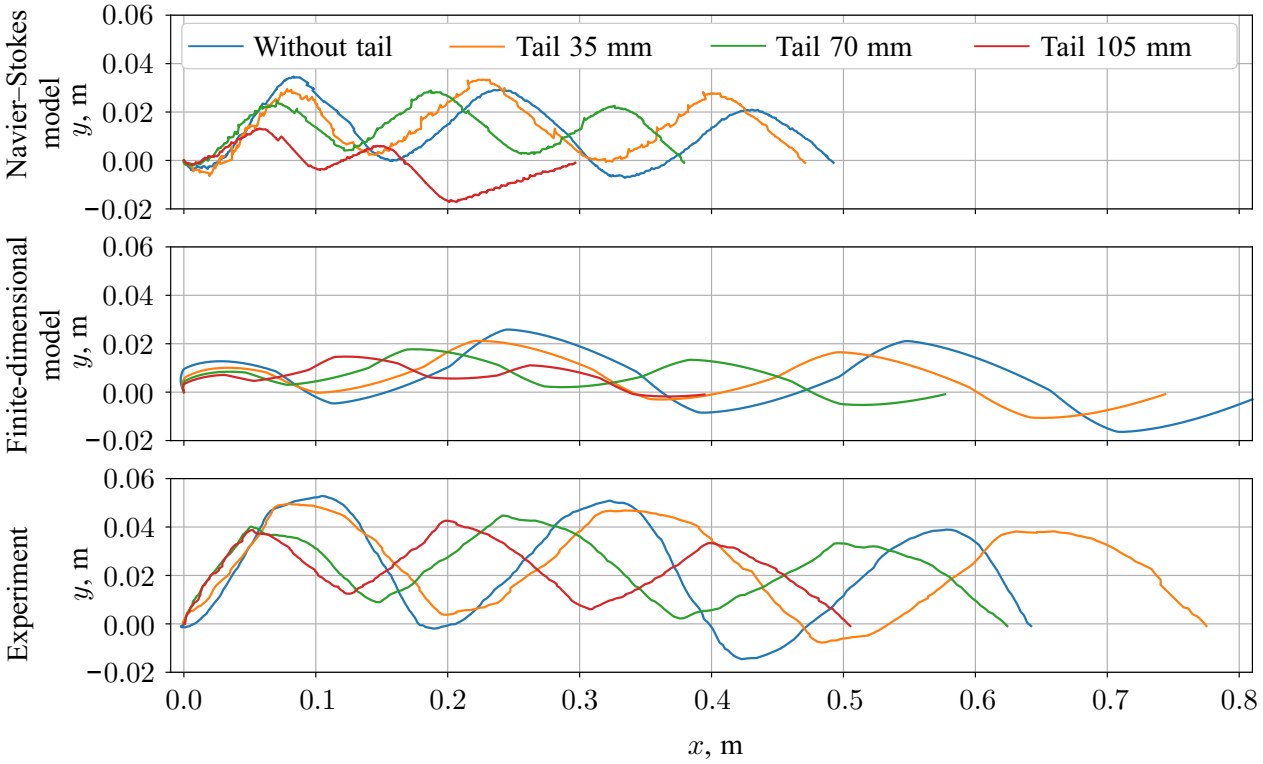

Fig. 13. Trajectories of the robot in the experiment and simulation with the period of control action $T = 3$ s for different tail fins

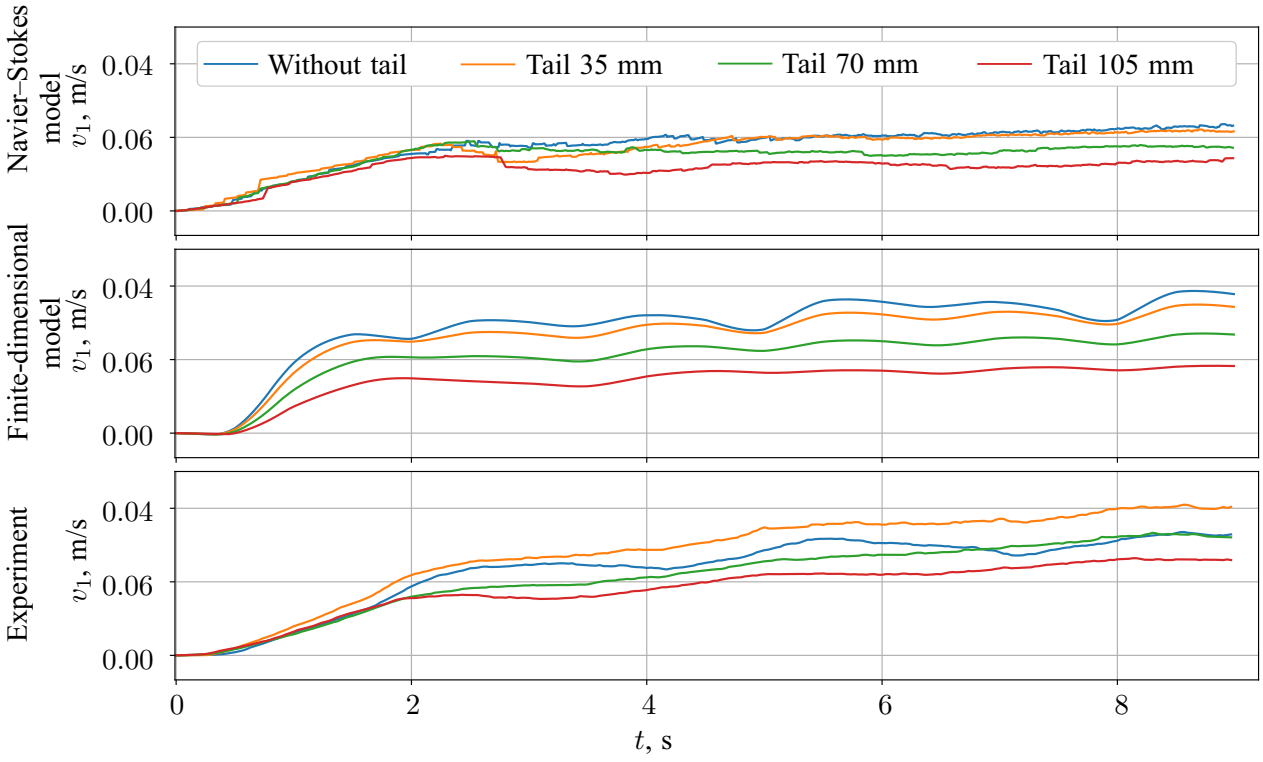

Fig. 14. Linear velocities of the robot in the experiment and simulations with the period of control action $T = 3$ s for different tail fins

experiment within a small computation time, and the calculations from the model based on the Navier–Stokes equations are very time-consuming. For simulations, we used periods of the control signal from 1 to 8 seconds with a step of 0.1 s. Figure 15 shows graphs of the average steady-state linear velocity for the corresponding control period in the experiments and simulations.

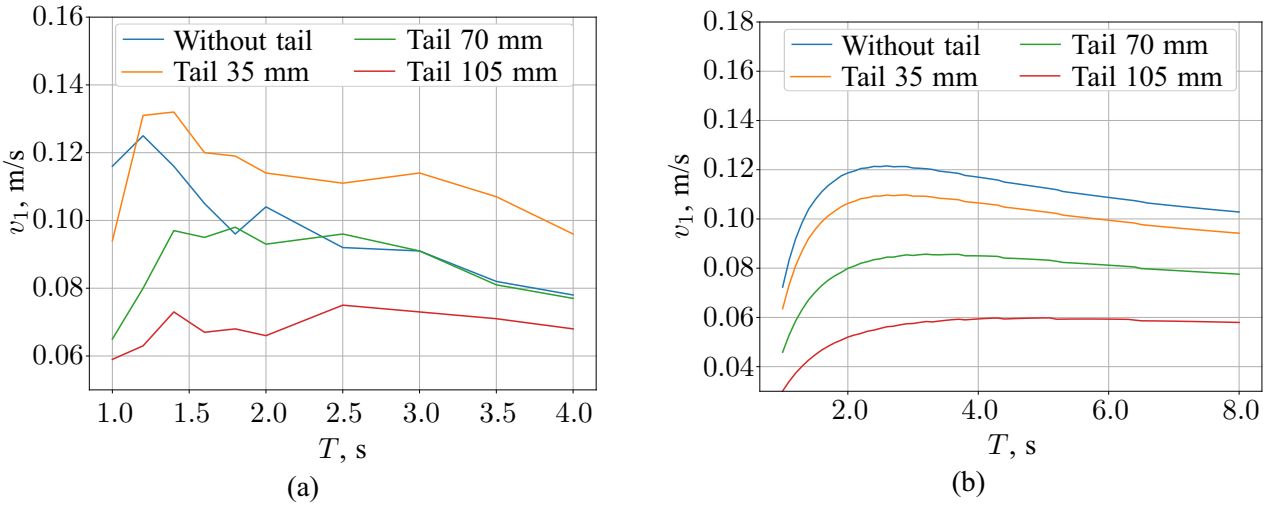

Fig. 15. The steady-state linear velocity in the longitudinal direction for different tails depending on the period of control action: a) of the real prototype; b) of the finite-dimensional model

From the graphs in Fig. 15 it can be seen that the maximal velocity is guaranteed by the set of values of the tail length and the control period. It is interesting that, with increasing control period, the velocity of motion with a tail fin observed in the experiments exceeded the velocity of motion without a tail fin. In the simulations (using a finite-dimensional model) this phenomenon was not observed.

§ 4. Conclusion

In this work we have developed two mathematical models of robot motion in a fluid: a finite-dimensional model, based on the Kirchhoff equations for the motion of a rigid body in a fluid, and a model based on the Navier–Stokes equations. To compare and test the simulation results, we have developed and created a prototype of the aquatic robot with a spinning rotor, with which real experiments have been conducted. The results obtained suggest the following conclusions.

1. The mathematical models have no quantitative exact agreement with experiment. However, using the finite-dimensional model, we obtained solutions that exhibit a better fit to the experimental data than those obtained using the mathematical model based on the Navier–Stokes equations. But the scope of applicability of this finite-dimensional model requires additional studies. The discrepancy between the model of the Navier–Stokes equations and the real experiment suggests that the two-dimensional formulation of the problem does not take into account all phenomena that occur and influence the propulsion of the object in the real experiment. Possibly, the solution in a three-dimensional formulation of the problem will show results that will be closer to those of the experiment, but the complexity of the model will noticeably increase in this case. Such models can be used at the stage of designing prototypes and planning further studies, however, they are not suitable to construct control systems.

2. Adding a rigid tail fin to the robot body over small control periods (high oscillation frequencies of the rotor) leads to no increase in the efficiency of motion. On the contrary, a converse effect manifests itself. However, with increasing control period (with decreasing

oscillation frequency of the rotor) the maximal velocity that is developed by the robot with rigid tail fins can exceed the maximal velocity developed by the robot without a tail fin. This effect is well noticeable in the experiment, and in the simulation based on the Navier–Stokes equations this effect is not so pronounced, but is still present. In this simulation with control period $T = 1.2$ s the velocity of the robot without a tail fin exceeds the velocity with any tail almost throughout the motion, but with control period $T = 3$ s the velocity of the robot without a tail fin is similar to the velocity of the robot with a tail fin of length 35 mm.

3. From the experiments it can also be seen that for each tail fin there is some value of the period of the control signal for which the maximal velocity of motion with this tail fin is achieved. This effect is also confirmed in both mathematical models.

In previous work, a robot with two rotating eccentrics inside the robot body and with flexible tail fins [24] was considered and it was shown that the flexible tail fin can significantly increase the velocity of propulsion of objects in a fluid, namely, by a factor of 5 to 10. This implies that the propulsion is influenced to a greater extent by the rigidity of the fin rather than by its length. It can be assumed that for specific flexible tail fins also there exists an optimal oscillation frequency of the rotor with which the robot will develop the maximal velocity for this tail fin.

4. The form of the robot's trajectory obtained from the finite-dimensional model is greatly influenced by parameters such as the coefficients of viscous resistance and added masses. Their theoretical calculation for objects with complex form which move near the free surface is a fairly labor-intensive problem. Therefore, much of recent work [18, 19, 38, 42, 43] to simulate the motion of robots moving in aqueous media involves calculation of the model's parameters by using experimental data. This approach enables a quantitative agreement between the finite-dimensional model and the experiment, but the question arises of the scope of application of this model for different modes of motion. It is the choice (calculation) of these coefficients that is one of the important factors that influence the adequacy of the mathematical models featuring the motion of objects in a fluid without solving the Navier–Stokes equations. If under the operation conditions under consideration the finite-dimensional model provides at least a qualitatively correct description of the motion pattern of the robot, it can be used both to optimize the design and to develop new control algorithms or to modify the existing control algorithms, in particular, in real time.

5. As various robots move in a liquid medium, whether it be fishlike objects or objects controlled by internal masses, which are discussed in this paper, vortices are formed and fluid circulation occurs near the object, which also contributes to the motion (note that the contribution can be both positive and negative). If we assume that during the periodic motion of the airfoil (with an additional tail fin or without it) the arising fluid circulation contributes to propulsion, then the method for accounting this contribution in the finite-dimensional model would be to add some delay in control to the equations of motion [38, 41], which can improve the agreement between the simulated trajectories and the experimental ones.

Funding. This work is supported by the Russian Science Foundation under grant 25–11–00305.

REFERENCES

1. Arnol'd V. I., Kozlov V. V., Neishtadt A. I. Mathematical aspects of classical and celestial mechanics, *Itogi Nauki i Tekhniki. Seriya "Sovremennye Problemy Matematiki. Fundamental'nye Napravleniya"*, 1985, vol. 3, pp. 5–290. https://www.mathnet.ru/eng/intf28
2. Borisov A. V., Kuznetsov S. P., Mamaev I. S., Tenenev V. A. Describing the motion of a body with an elliptical cross section in a viscous uncompressible fluid by model equations reconstructed from data processing, *Technical Physics Letters*, 2016, vol. 42, no. 9, pp. 886–890. https://doi.org/10.1134/S1063785016090042

3. Borisov A. V., Mamaev I. S., Vetchanin E. V. Self-propulsion of a smooth body in a viscous fluid under periodic oscillations of a rotor and circulation, *Regular and Chaotic Dynamics*, 2018, vol. 23, nos. 7–8, pp. 850–874. https://doi.org/10.1134/S1560354718070043
4. Chernous'ko F. L. Motion of a body in a fluid due to attached-link oscillations, *Doklady Physics*, 2010, vol. 55, no. 3, pp. 138–141. https://doi.org/10.1134/s1028335810030080
5. Chernousko F., Bolotnik N. *Dynamics of mobile systems with controlled configuration*, Singapore: Springer, 2024. https://doi.org/10.1007/978-981-97-1825-2
6. Childress S., Spagnolie S. E., Tokieda T. A bug on a raft: recoil locomotion in a viscous fluid, *Journal of Fluid Mechanics*, 2011, vol. 669, pp. 527–556. https://doi.org/10.1017/S002211201000515X
7. Chivkula P., Tallapragada P. A vibration driven slender elastic swimmer, *APS Division of Fluid Dynamics (Fall)*, 2024, abstract id A06.006. https://ui.adsabs.harvard.edu/abs/2024APS..DFDA06006C/abstract
8. Chivkula P., Tallapragada P. Spin swimmer: a fast, efficient and agile fish-like robot, *IEEE Robotics and Automation Letters*, 2025, vol. 10, issue 10, pp. 10942–10949. https://doi.org/10.1109/LRA.2025.3606357
9. Chu Won-Shik, Lee Kyung-Tae, Song Sung-Hyuk, Han Min-Woo, Lee Jang-Yeob, Kim Hyung-Soo, Kim Min-Soo, Park Yong-Jai, Cho Kyu-Jin, Ahn Sung-Hoon. Review of biomimetic underwater robots using smart actuators, *International Journal of Precision Engineering and Manufacturing*, 2012, vol. 13, no. 7, pp. 1281–1292. https://doi.org/10.1007/s12541-012-0171-7
10. Dosaev M., Golovanov S., Klimina L., Selyutskiy Y. Serpentine motion of a trimaran robot, *Proceedings of the Institution of Mechanical Engineers, Part C: Journal of Mechanical Engineering Science*, 2023, vol. 238, no. 3, pp. 737–745. https://doi.org/10.1177/09544062231186967
11. Free B. A., Lee Jinseong, Paley D. A. Bioinspired pursuit with a swimming robot using feedback control of an internal rotor, *Bioinspiration and Biomimetics*, 2020, vol. 15, no. 3, 035005. https://doi.org/10.1088/1748-3190/ab745e
12. Galdi G. P. On the self-propulsion of a rigid body in a viscous liquid by time-periodic boundary data, *Journal of Mathematical Fluid Mechanics*, 2020, vol. 22, no. 4, article number: 61. https://doi.org/10.1007/s00021-020-00537-z
13. Galdi G. P., Karakouzian M. M. On the propulsion of a rigid body in a viscous liquid under the action of a time-periodic force, *Research in the Mathematical Sciences*, 2025, vol. 12, article number: 31. https://doi.org/10.1007/s40687-025-00510-0
14. Hoerner S. F. *Fluid-dynamic drag*, New York: Hoerner Fluid Dynamics, 1965.
15. Journée J. M. J., Massie W. W. *Offshore hydromechanics*, Delft: Delft University of Technology, 2001.
16. Karavaev Yu. L., Kilin A. A., Klekovkin A. V. Experimental investigations of the controlled motion of a screwless underwater robot, *Regular and Chaotic Dynamics*, 2016, vol. 21, nos. 7–8, pp. 918–926. https://doi.org/10.1134/S1560354716070133
17. Karavaev Yu. L., Klekovkin A. V., Mamaev I. S., Tenenev V. A., Vetchanin E. V. A simple physical model for control of a propellerless aquatic robot, *Journal of Mechanisms and Robotics*, 2022, vol. 14, issue 1, 011007. https://doi.org/10.1115/1.4051240
18. Kelasidi E., Pettersen K. Y., Gravdahl J. T., Liljebäck P. Modeling of underwater snake robots, *2014 IEEE International Conference on Robotics and Automation (ICRA)*, IEEE, 2014, pp. 4540–4547. https://doi.org/10.1109/ICRA.2014.6907522
19. Kelasidi E., Liljebäck P., Pettersen K. Y., Gravdahl J. T. Innovation in underwater robots: Biologically inspired swimming snake robots, *IEEE Robotics and Automation Magazine*, 2016, vol. 23, issue 1, pp. 44–62. https://doi.org/10.1109/MRA.2015.2506121
20. Kilin A. A., Klenov A. I., Tenenev V. A. Controlling the movement of the body using internal masses in a viscous liquid, *Computer Research and Modeling*, 2018, vol. 10, no. 4, pp. 445–460 (in Russian). https://doi.org/10.20537/2076-7633-2018-10-4-445-460
21. Kilin A. A., Gavrilova A. M., Artemova E. M. Dynamics of an elliptic foil with an attached vortex in an ideal fluid: The integrable case, *Regular and Chaotic Dynamics*, 2025, vol. 30, no. 6, pp. 931–951. https://doi.org/10.1134/S1560354724590015

22. Klekovkin A. V. Simulation of the motion of a propellerless mobile robot controlled by rotation of the internal rotor, *Vestnik Udmurtskogo Universiteta. Matematika. Mekhanika. Komp'yuternye Nauki*, 2020, vol. 30, issue 4, pp. 645–656 (in Russian). https://doi.org/10.35634/vm200408
23. Klekovkin A. V., Karavaev Yu. L., Mamaev I. S. The control of an aquatic robot by a periodic rotation of the internal flywheel, *Russian Journal of Nonlinear Dynamics*, 2023, vol. 19, no. 2, pp. 265–279. https://doi.org/10.20537/nd230301
24. Klekovkin A. V., Karavaev Yu. L., Kilin A. A., Nazarov A. V. The influence of tail fins on the speed of an aquatic robot driven by internal moving masses, *Computer Research and Modeling*, 2024, vol. 16, no. 4, pp. 869–882 (in Russian). https://doi.org/10.20537/2076-7633-2024-16-4-869-882
25. Klenov A. I., Kilin A. A. Influence of vortex structures on the controlled motion of an above-water screwless robot, *Regular and Chaotic Dynamics*, 2016, vol. 21, nos. 7–8, pp. 927–938. https://doi.org/10.1134/S1560354716070145
26. Klimina L. A., Golovanov S. A., Dosaev M. Z., Selyutskiy Y. D., Holub A. P. Plane-parallel motion of a trimaran capsubot controlled with an internal flywheel, *International Journal of Non-Linear Mechanics*, 2023, vol. 150, 104341. https://doi.org/10.1016/j.ijnonlinmec.2022.104341
27. Koiri M. K., Sharma A. K., Jha A., Kumar J. A comprehensive review of bio-inspired swimming in robotic fishes, *Sensors and Actuators A: Physical*, 2025, vol. 394, 116913. https://doi.org/10.1016/j.sna.2025.116913
28. Kopysov S. P., Tonkov L. E., Chernova A. A. Two-way coupling simulation of interaction between a supersonic flow and a non-rigid plate. Comparison of numerical and experimental results, *Computational Continuum Mechanics*, 2013, vol. 6, no. 1, pp. 78–85 (in Russian). https://doi.org/10.7242/1999-6691/2013.6.1.10
29. Korotkin A. I. *Added masses of ship structures*, Dordrecht: Springer, 2009. https://doi.org/10.1007/978-1-4020-9432-3
30. Kozlov V. V., Ramodanov S. M. The motion of a variable body in an ideal fluid, *Journal of Applied Mathematics and Mechanics*, 2001, vol. 65, issue 4, pp. 579–587. https://doi.org/10.1016/S0021-8928(01)00063-6
31. Kozlov V. V., Onishchenko D. A. The motion in a perfect fluid of a body containing a moving point mass, *Journal of Applied Mathematics and Mechanics*, 2003, vol. 67, issue 4, pp. 553–564. https://doi.org/10.1016/S0021-8928(03)90058-X
32. Newman J. N. *Marine hydrodynamics*, Cambridge, MA: The MIT Press, 2017.
33. Pollard B., Tallapragada P. An aquatic robot propelled by an internal rotor, *IEEE/ASME Transactions on Mechatronics*, 2017, vol. 22, issue 2, pp. 931–939. https://doi.org/10.1109/TMECH.2016.2630998
34. Qin Y., Zhang Z. Y., Sha W. H., Sun R. Self-propulsion of a submerged sphere due to coupling of its deformation and internal mass shift, *Physics of Fluids*, 2022, vol. 34, issue 4, 047120. https://doi.org/10.1063/5.0086736
35. Ramodanov S. M., Tenenev V. A. Motion of a body with variable distribution of mass in a boundless viscous liquid, *Russian Journal of Nonlinear Dynamics*, 2011, vol. 7, no. 3, pp. 635–647 (in Russian). https://doi.org/10.20537/nd1103016
36. Simo J. C., Wong K. K. Unconditionally stable algorithms for rigid body dynamics that exactly preserves energy and momentum, *International Journal for Numerical Methods in Engineering*, 1991, vol. 31, issue 1, pp. 19–52. https://doi.org/10.1002/nme.1620310103
37. Trottenberg U., Oosterlee C. W., Schuller A. *Multigrid*, London: Academic Press, 2000.
38. Verma S., Xu Jian-Xin. Data-assisted modeling and speed control of a robotic fish, *IEEE Transactions on Industrial Electronics*, 2017, vol. 64, issue 5, pp. 4150–4157. https://doi.org/10.1109/TIE.2016.2613500
39. Vetchanin E. V., Kilin A. A. Free and controlled motion of a body with a moving internal mass through a fluid in the presence of circulation around the body, *Doklady Physics*, 2016, vol. 61, no. 1, pp. 32–36. https://doi.org/10.1134/S1028335816010110
40. Vetchanin E. V., Mamaev I. S. Numerical analysis of the periodic controls of an aquatic robot, *Vestnik Udmurtskogo Universiteta. Matematika. Mekhanika. Komp'yuternye Nauki*, 2022, vol. 32, issue 4, pp. 644–660 (in Russian). https://doi.org/10.35634/vm220410

41. Vetchanin E. V., Valieva A. R. Analysis of the force and torque arising during the oscillatory motion of a Joukowsky foil in a fluid, *Russian Journal of Nonlinear Dynamics*, 2024, vol. 20, no. 1, pp. 79–93. https://doi.org/10.20537/nd231210
42. Wang Jianxun, Tan Xiaobo. A dynamic model for tail-actuated robotic fish with drag coefficient adaptation, *Mechatronics*, 2013, vol. 23, issue 6, pp. 659–668. https://doi.org/10.1016/j.mechatronics.2013.07.005
43. Wang Yang Wei, Tan Jin Bo, Gu Bao Tong, Sang Peng Fei, Zhao Dong Biao. Design and modeling of a biomimetic stingray-like robotic fish, *Advanced Materials Research*, 2014, vol. 945–949, pp. 1473–1477. https://doi.org/10.4028/www.scientific.net/AMR.945-949.1473
44. Yegorov A. G., Zakharova O. S. The energy-optimal motion of a vibration-driven robot in a resistive medium, *Journal of Applied Mathematics and Mechanics*, 2010, vol. 74, issue 4, pp. 443–451. https://doi.org/10.1016/j.jappmathmech.2010.09.010
45. Zhong Yong, Hong Zicun, Li Yuhan, Yu Junzhi. A general kinematic model of fish locomotion enables robot fish to master multiple swimming motions, *IEEE Transactions on Robotics*, 2024, vol. 40, pp. 750–763. https://doi.org/10.1109/TRO.2023.3339015

Received 26.09.2025
Accepted 29.11.2025

Anton Vladimirovich Klekovkin, Candidate of Engineering, Senior Researcher, Kalashnikov Izhevsk State Technical University, ul. Studencheskaya, 7, Izhevsk, 426069, Russia.
ORCID: https://orcid.org/0000-0002-8483-1332
E-mail: a.v.klekovkin@istu.ru

Alena Alekseevna Chernova, Doctor of Engineering, Associate Professor, Chief Researcher, Kalashnikov Izhevsk State Technical University, ul. Studencheskaya, 7, Izhevsk, 426069, Russia.
ORCID: https://orcid.org/0000-0001-8579-6279
E-mail: a.a.chernova@istu.ru

Yury Leonidovich Karavaev, Doctor of Engineering, Associate Professor, Leading Researcher, Kalashnikov Izhevsk State Technical University, ul. Studencheskaya, 7, Izhevsk, 426069, Russia.
ORCID: https://orcid.org/0000-0002-6679-1293
E-mail: karavaev_yury@istu.ru

Anton Vyacheslavovich Nazarov, Research Engineer, Kalashnikov Izhevsk State Technical University, ul. Studencheskaya, 7, Izhevsk, 426069, Russia.
ORCID: https://orcid.org/0009-0001-1824-210X
E-mail: antonnaz14@gmail.com

Citation: A. V. Klekovkin, A. A. Chernova, Yu. L. Karavaev, A. V. Nazarov. Investigation of the motion of an aquatic robot with an internal fast-speed rotor and a nondeformable tail fin, *Vestnik Udmurtskogo Universiteta. Matematika. Mekhanika. Komp'yuternye Nauki*, 2025, vol. 35, issue 4, pp. 619–642.

МЕХАНИКА 2025. Т. 35. Вып. 4. С. 619–642.

А. В. Клековкин, А. А. Чернова, Ю. Л. Караваев, А. В. Назаров

Исследование движения водного робота с внутренним быстровращающимся ротором и недеформируемым хвостовым плавником

Ключевые слова: водный робот, численное моделирование, конечномерная модель, экспериментальные исследования.

УДК 531.36, 532.54, 517.95

DOI: 10.35634/vm250407

В данной работе проведено моделирование движения водного робота с внутренним быстровращающимся ротором. Разработаны две математические модели движения робота в жидкости: модель движения основанная на уравнениях Кирхгофа для движения твердого тела в жидкости и модель, основанная на уравнениях Навье–Стокса. Помимо моделирования создан прототип водного робота с быстровращающимся ротором, с которым проведены реальные эксперименты. В работе представлены результаты реальных экспериментов и моделирования, сделаны выводы.

Финансирование. Исследования выполнены в рамках гранта Российского научного фонда № 25–11–00305.

СПИСОК ЛИТЕРАТУРЫ

1. Арнольд В. И., Козлов В. В., Нейштадт А. И. Математические аспекты классической и небесной механики // Итоги науки и техники. Серия «Современные проблемы математики. Фундаментальные направления». 1985. Т. 3. С. 5–290. https://www.mathnet.ru/rus/intf28
2. Борисов А. В., Кузнецов С. П., Мамаев И. С., Тененев В. А. Описание движения тела эллиптического сечения в вязкой несжимаемой жидкости с помощью модельных уравнений, реконструированных на основе обработки данных // Письма в журнал технической физики. 2016. Т. 42. № 17. С. 9–19. https://www.elibrary.ru/item.asp?id=27368304
3. Borisov A. V., Mamaev I. S., Vetchanin E. V. Self-propulsion of a smooth body in a viscous fluid under periodic oscillations of a rotor and circulation // Regular and Chaotic Dynamics. 2018. Vol. 23. Nos. 7–8. P. 850–874. https://doi.org/10.1134/S1560354718070043
4. Черноусько Ф. Л. О перемещении тела в жидкости за счет колебаний присоединенного звена // Доклады Академии наук. 2010. Т. 431. № 1. С. 46–49. https://www.elibrary.ru/item.asp?id=13726950
5. Chernousko F., Bolotnik N. Dynamics of mobile systems with controlled configuration. Singapore: Springer, 2024. https://doi.org/10.1007/978-981-97-1825-2
6. Childress S., Spagnolie S. E., Tokieda T. A bug on a raft: recoil locomotion in a viscous fluid // Journal of Fluid Mechanics. 2011. Vol. 669. P. 527–556. https://doi.org/10.1017/S002211201000515X
7. Chivkula P., Tallapragada P. A vibration driven slender elastic swimmer // APS Division of Fluid Dynamics (Fall). 2024. Abstract ID A06.006. https://ui.adsabs.harvard.edu/abs/2024APS..DFDA06006C/abstract
8. Chivkula P., Tallapragada P. Spin swimmer: a fast, efficient and agile fish-like robot // IEEE Robotics and Automation Letters. 2025. Vol. 10. Issue 10. P. 10942–10949. https://doi.org/10.1109/LRA.2025.3606357
9. Chu Won-Shik, Lee Kyung-Tae, Song Sung-Hyuk, Han Min-Woo, Lee Jang-Yeob, Kim Hyung-Soo, Kim Min-Soo, Park Yong-Jai, Cho Kyu-Jin, Ahn Sung-Hoon. Review of biomimetic underwater robots using smart actuators // International Journal of Precision Engineering and Manufacturing. 2012. Vol. 13. No. 7. P. 1281–1292. https://doi.org/10.1007/s12541-012-0171-7
10. Dosaev M., Golovanov S., Klimina L., Selyutskiy Y. Serpentine motion of a trimaran robot // Proceedings of the Institution of Mechanical Engineers, Part C: Journal of Mechanical Engineering Science. 2023. Vol. 238. No. 3. P. 737–745. https://doi.org/10.1177/09544062231186967

11. Free B. A., Lee Jinseong, Paley D. A. Bioinspired pursuit with a swimming robot using feedback control of an internal rotor // Bioinspiration and Biomimetics. 2020. Vol. 15. No. 3. 035005. https://doi.org/10.1088/1748-3190/ab745e
12. Galdi G. P. On the self-propulsion of a rigid body in a viscous liquid by time-periodic boundary data // Journal of Mathematical Fluid Mechanics. 2020. Vol. 22. No. 4. Article number: 61. https://doi.org/10.1007/s00021-020-00537-z
13. Galdi G. P., Karakouzian M. M. On the propulsion of a rigid body in a viscous liquid under the action of a time-periodic force // Research in the Mathematical Sciences. 2025. Vol. 12. Article number: 31. https://doi.org/10.1007/s40687-025-00510-0
14. Hoerner S. F. Fluid-dynamic drag. New York: Hoerner Fluid Dynamics, 1965.
15. Journée J. M. J., Massie W. W. Offshore hydromechanics. Delft: Delft University of Technology, 2001.
16. Karavaev Yu. L., Kilin A. A., Klekovkin A. V. Experimental investigations of the controlled motion of a screwless underwater robot // Regular and Chaotic Dynamics. 2016. Vol. 21. Nos. 7–8. P. 918–926. https://doi.org/10.1134/S1560354716070133
17. Karavaev Yu. L., Klekovkin A. V., Mamaev I. S., Tenenev V. A., Vetchanin E. V. A simple physical model for control of an propellerless aquatic robot // Journal of Mechanisms and Robotics. 2022. Vol. 14. Issue 1. 011007. https://doi.org/10.1115/1.4051240
18. Kelasidi E., Pettersen K. Y., Gravdahl J. T., Liljebäck P. Modeling of underwater snake robots // 2014 IEEE International Conference on Robotics and Automation (ICRA). IEEE, 2014. P. 4540–4547. https://doi.org/10.1109/ICRA.2014.6907522
19. Kelasidi E., Liljebäck P., Pettersen K. Y., Gravdahl J. T. Innovation in underwater robots: Biologically inspired swimming snake robots // IEEE Robotics and Automation Magazine. 2016. Vol. 23. Issue 1. P. 44–62. https://doi.org/10.1109/MRA.2015.2506121
20. Килин А. А., Кленов А. И., Тененев В. А. Управление движением тела с помощью внутренних масс в вязкой жидкости // Компьютерные исследования и моделирование. 2018. Т. 10. № 4. С. 445–460. https://doi.org/10.20537/2076-7633-2018-10-4-445-460
21. Kilin A. A., Gavrilova A. M., Artemova E. M. Dynamics of an elliptic foil with an attached vortex in an ideal fluid: The integrable case // Regular and Chaotic Dynamics. 2025. Vol. 30. No. 6. P. 931–951. https://doi.org/10.1134/S1560354724590015
22. Клековкин А. В. Моделирование движения безвинтового мобильного робота с неизменяемой формой оболочки управляемого с помощью вращения внутреннего ротора // Вестник Удмуртского университета. Математика. Механика. Компьютерные науки. 2020. Т. 30. Вып. 4. С. 645–656. https://doi.org/10.35634/vm200408
23. Klekovkin A. V., Karavaev Yu. L., Mamaev I. S. The control of an aquatic robot by a periodic rotation of the internal flywheel // Russian Journal of Nonlinear Dynamics. 2023. Vol. 19. No. 2. P. 265–279. https://doi.org/10.20537/nd230301
24. Клековкин А. В., Караваев Ю. Л., Килин А. А., Назаров А. В. Влияние хвостовых плавников на скорость водного робота, приводимого в движение внутренними подвижными массами // Компьютерные исследования и моделирование. 2024. Т. 16. № 4. С. 869–882. https://doi.org/10.20537/2076-7633-2024-16-4-869-882
25. Klenov A. I., Kilin A. A. Influence of vortex structures on the controlled motion of an above-water screwless robot // Regular and Chaotic Dynamics. 2016. Vol. 21. Nos. 7–8. P. 927–938. https://doi.org/10.1134/S1560354716070145
26. Klimina L. A., Golovanov S. A., Dosaev M. Z., Selyutskiy Y. D., Holub A. P. Plane-parallel motion of a trimaran capsubot controlled with an internal flywheel // International Journal of Non-Linear Mechanics. 2023. Vol. 150. 104341. https://doi.org/10.1016/j.ijnonlinmec.2022.104341
27. Koiri M. K., Sharma A. K., Jha A., Kumar J. A comprehensive review of bio-inspired swimming in robotic fishes // Sensors and Actuators A: Physical. 2025. Vol. 394. 116913. https://doi.org/10.1016/j.sna.2025.116913

28. Копысов С. П., Тонков Л. Е., Чернова А. А. Двухстороннее связывание при моделировании взаимодействия сверхзвукового потока и деформируемой пластины. Сравнение численных схем и результатов эксперимента // Вычислительная механика сплошных сред. 2013. Т. 6. № 1. С. 78–85. https://doi.org/10.7242/1999-6691/2013.6.1.10
29. Короткин А. И. Присоединенные массы судостроительных конструкций. СПб.: Мор Вест, 2007.
30. Козлов В. В., Рамоданов С. М. О движении изменяемого тела в идеальной жидкости // Прикладная математика и механика. 2001. Т. 65. Вып. 4. С. 592–601.
31. Козлов В. В., Онищенко Д. А. О движении в идеальной жидкости тела, содержащего внутри себя подвижную сосредоточенную массу // Прикладная математика и механика. 2003. Т. 67. Вып. 4. С. 620–633. https://www.elibrary.ru/item.asp?id=17296427
32. Newman J. N. Marine hydrodynamics. Cambridge, MA: The MIT Press, 2017.
33. Pollard B., Tallapragada P. An aquatic robot propelled by an internal rotor // IEEE/ASME Transactions on Mechatronics. 2017. Vol. 22. Issue 2. P. 931–939. https://doi.org/10.1109/TMECH.2016.2630998
34. Qin Y., Zhang Z. Y., Sha W. H., Sun R. Self-propulsion of a submerged sphere due to coupling of its deformation and internal mass shift // Physics of Fluids. 2022. Vol. 34. Issue 4. 047120. https://doi.org/10.1063/5.0086736
35. Рамоданов С. М., Тененев В. А. Движение тела с переменной геометрией масс в безграничной вязкой жидкости // Нелинейная динамика. 2011. Т. 7. № 3. С. 635–647. https://doi.org/10.20537/nd1103016
36. Simo J. C., Wong K. K. Unconditionally stable algorithms for rigid body dynamics that exactly preserves energy and momentum // International Journal for Numerical Methods in Engineering. 1991. Vol. 31. Issue 1. P. 19–52. https://doi.org/10.1002/nme.1620310103
37. Trottenberg U., Oosterlee C. W., Schuller A. Multigrid. London: Academic Press, 2000.
38. Verma S., Xu Jian-Xin. Data-assisted modeling and speed control of a robotic fish // IEEE Transactions on Industrial Electronics. 2017. Vol. 64. Issue 5. P. 4150–4157. https://doi.org/10.1109/TIE.2016.2613500
39. Ветчанин Е. В., Килин А. А. Свободное и управляемое движение в жидкости тела с подвижной внутренней массой при наличии циркуляции вокруг тела // Доклады Академии наук. 2016. Т. 466. № 3. С. 293–297. https://doi.org/10.7868/S0869565216030129
40. Ветчанин Е. В., Мамаев И. С. Численный анализ периодических управлений водного робота неизменной формы // Вестник Удмуртского университета. Математика. Механика. Компьютерные науки. 2022. Т. 32. Вып. 4. С. 644–660. https://doi.org/10.35634/vm220410
41. Vetchanin E. V., Valieva A. R. Analysis of the force and torque arising during the oscillatory motion of a Joukowsky foil in a fluid // Russian Journal of Nonlinear Dynamics. 2024. Vol. 20. No. 1. P. 79–93. https://doi.org/10.20537/nd231210
42. Wang Jianxun, Tan Xiaobo. A dynamic model for tail-actuated robotic fish with drag coefficient adaptation // Mechatronics. 2013. Vol. 23. Issue 6. P. 659–668. https://doi.org/10.1016/j.mechatronics.2013.07.005
43. Wang Yang Wei, Tan Jin Bo, Gu Bao Tong, Sang Peng Fei, Zhao Dong Biao. Design and modeling of a biomimetic stingray-like robotic fish // Advanced Materials Research. 2014. Vol. 945–949. P. 1473–1477. https://doi.org/10.4028/www.scientific.net/AMR.945-949.1473
44. Егоров А. Г., Захарова О. С. Оптимальное по энергетическим затратам движение виброробота в среде с сопротивлением // Прикладная математика и механика. 2010. Т. 74. Вып. 4. С. 620–632. https://www.elibrary.ru/item.asp?id=15140200
45. Zhong Yong, Hong Zicun, Li Yuhan, Yu Junzhi. A general kinematic model of fish locomotion enables robot fish to master multiple swimming motions // IEEE Transactions on Robotics. 2024. Vol. 40. P. 750–763. https://doi.org/10.1109/TRO.2023.3339015

Поступила в редакцию 26.09.2025
Принята к публикации 29.11.2025

Клековкин Антон Владимирович, к. т. н., старший научный сотрудник, Ижевский государственный технический университет имени М. Т. Калашникова, 426069, Россия, г. Ижевск, ул. Студенческая, 7.
ORCID: https://orcid.org/0000-0002-8483-1332
E-mail: a.v.klekovkin@istu.ru

Чернова Алена Алексеевна, д. т. н., доцент, главный научный сотрудник, Ижевский государственный технический университет имени М. Т. Калашникова, 426069, Россия, г. Ижевск, ул. Студенческая, 7.
ORCID: https://orcid.org/0000-0001-8579-6279
E-mail: a.a.chernova@istu.ru

Караваев Юрий Леонидович, д. т. н., доцент, ведущий научный сотрудник, Ижевский государственный технический университет имени М. Т. Калашникова, 426069, Россия, г. Ижевск, ул. Студенческая, 7.
ORCID: https://orcid.org/0000-0002-6679-1293
E-mail: karavaev_yury@istu.ru

Назаров Антон Вячеславович, инженер-исследователь, Ижевский государственный технический университет имени М. Т. Калашникова, 426069, Россия, г. Ижевск, ул. Студенческая, 7.
ORCID: https://orcid.org/0009-0001-1824-210X
E-mail: antonnaz14@gmail.com

Цитирование: А. В. Клековкин, А. А. Чернова, Ю. Л. Караваев, А. В. Назаров. Исследование движения водного робота с внутренним быстровращающимся ротором и недеформируемым хвостовым плавником // Вестник Удмуртского университета. Математика. Механика. Компьютерные науки. 2025. Т. 35. Вып. 4. С. 619–642.